Geissman, S. J. Reynolds, *Nature* **361**, 56 (1993).
4. G. S. Lister and S. L. Baldwin, *Geology* **21**, 607 (1993); T. Parsons and G. A. Thompson, *ibid.*, p. 247.
5. R. W. Allmendinger *et al.*, *ibid.* **11**, 532 (1983); D. B. von Tish, R. W. Allmendinger, J. W. Sharp, *Am. Assoc. Pet. Geol. Bull.* **69**, 1077 (1985).
6. R. B. Smith and R. L. Bruhn, *J. Geophys. Res.* **89**, 5733 (1984).
7. D. S. Coleman, thesis, University of Kansas (1991).
8. J. D. Walker and J. M. Bartley, in preparation.
9. M. N. Machette and T. A. Steven, *U.S. Geol. Surv. Mis. Invest. Map I-1455* (1983).
10. D. L. Nielson *et al.*, *Geology of Roosevelt Hot Springs KGRA, Beaver County, Utah* (Earth Science Laboratory, University of Utah Research Institute, Salt Lake City, 1978).
11. B. S. Sibbett and D. L. Nielson, *Geology of the Central Mineral Mountains, Beaver County, Utah* (Earth Sciences Laboratory Rep. 33, Utah University Research Institute, Salt Lake City, 1980).
12. D. L. Nielson, S. H. Evans, B. S. Sibbett, *Geol. Soc. Am. Bull.* **97**, 765 (1986).
13. J. N. Aleinikoff, D. L. Nielson, C. E. Hedge, S. H. Evans, *U.S. Geol. Surv. Bull. 1622* (1987).
14. D. S. Coleman and J. D. Walker, *J. Geophys. Res.* **92**, 11011 (1992).
15. D. E. Price and J. M. Bartley, *Geol. Soc. Am. Rocky Mtn. Sect. Abstr. Progr.* **24**, 58 (1992).
16. D. E. Price and J. M. Bartley, *Geol. Soc. Am. Cord. Sect. Abstr. Progr.* **22**, 76 (1990).
17. H. C. Liese, thesis, University of Utah (1957).
18. T. A. Steven, C. G. Cunningham, C. W. Naeser, H. H. Menhert, *U.S. Geol. Surv. Bull.* **1469** (1979).
19. S. H. Evans, T. A. Stevens, *Geol. Soc. Am. Bull.* **93**, 1131 (1982).
20. D. S. Coleman, J. W. Geissman, J. D. Walker, *Eos* **72**, 468 (1991). D. S. Coleman and J. W. Geissman, in preparation.
21. All samples were hand-picked to remove impurities, air-abraded, loaded into dissolution vessels, spiked with a mixed ^{205}Pb:^{235}U:^{233}U spike and dissolved in an HF-HNO_3 mixture at 220°C (*22*). Separation of U and Pb was accomplished using standard HCl chemistry. Pb and U were loaded on single Re filaments; Pb in silica gel plus H_3PO_4, and U in carbon plus H_3PO_4. All analyses were performed on the VG Sector 54 thermal ionization mass spectrometer housed at MIT. Lead was analyzed either in single-collector ion-counting mode, or static multicollector mode with ^{204}Pb measured using ion-counting. Uranium was measured as a metal ion in static multicollector mode.
22. R. R. Parrish, *Chem. Geol.* **66**, 99 (1987).
23. Reported K-Ar ages for the rhyolite porphyry dikes (*12*) agree well with those for the Gillies Hill rhyolite (*19*). However, K-Ar dates for intrusive rocks from the Mineral Mountains are consistently younger than U-Pb dates for the same phases (*7, 13*), and therefore probably represent cooling ages. We accept the K-Ar age for the Gillies Hill rhyolite as a crystallization age because it was obtained from an extrusive rock.
24. S. H. Evans and D. L. Nielson, *Geotherm. Res. Council Trans.* **6**, 15 (1982).
25. Supported by National Science Foundation grant EAR-8904007 to J.D.W. and Geological Society of America and Sigma Xi grants to D.S.C. We thank J. Bartley, J. Geissman, J. D. R. Applegate, S. Bowring, J. Fletcher, and B. Wernicke for helpful discussions, S. Coleman for mapping and sample collection, K. Davidek for sample preparation, and two anonymous reviewers.

30 July 1993; accepted 24 November 1993

Turbulent Mixing Under Drifting Pack Ice in the Weddell Sea

Miles G. McPhee and Douglas G. Martinson

By providing cold, dense water that sinks and mixes to fill the abyssal world ocean, high-latitude air-sea-ice interaction is the main conduit through which the deep ocean communicates with the rest of the climate system. A key element in modeling and predicting oceanic impact on climate is understanding the processes that control the near surface exchange of heat, salt, and momentum. In 1992, the United States–Russian Ice Station Weddell-1 traversed the western Weddell Sea during the onset of winter, providing a platform for direct measurement of turbulent heat flux and Reynolds stress in the upper ocean. Data from a storm early in the drift indicated (i) well-formed Ekman spirals (in both velocity and turbulent stress); (ii) high correlation between mixed layer heat flux and temperature gradients; (iii) that eddy viscosity and eddy thermal diffusivity were similar, about 0.02 square meters per second; and (iv) that the significant turbulent length scale (2 to 3 meters through most of the boundary layer) was proportional to the wavelength at the peak in the weighted vertical velocity spectrum. The measurements were consistent with a simple model in which the bulk eddy viscosity in the neutrally buoyant mixed layer is proportional to kinematic boundary stress divided by the Coriolis parameter.

Despite widespread interest in understanding how turbulence from wind stress and energy exchange at the surface distributes momentum, heat, and salt in the upper part of the ocean (*1*), direct flux measurements in the oceanic boundary layer (OBL) are rare, mostly because of the difficulty of measuring small turbulent fluctuations and mean flow gradients in the presence of a vigorous surface wave field. A largely unmet goal of oceanic turbulence research is the relation of the turbulent flux of a quantity to its mean gradient by means of an eddy diffusivity (or eddy viscosity if the quantity is vector momentum) coefficient. Eddy diffusivity, which depends more on the characteristics of the turbulent flow than on the particular fluid, is presumed to play a role in distributing properties analogous to that of molecular diffusivity but is generally much larger in geophysical flows. The concept has obvious utility for the modeling of the response of the upper ocean to changes in wind stress or surface fluxes of heat and salt.

Drifting sea ice effectively damps most surface waves and provides a stable platform from which it is relatively easy to deploy instruments sensitive enough to measure turbulence. In 1992, we maintained such equipment at several levels under the United States–Russian Ice Station Weddell-1 (ISW-1) as it drifted north in a region of multiyear pack ice east of the Antarctic Peninsula (*2*). In this report, we combine our direct measurements of turbulent heat flux and Reynolds stress (*3*) with basic planetary boundary layer theory and temperature-gradient data to estimate eddy viscosity and eddy thermal diffusivity. We also investigate the dominant length scale in the turbulent transfer process and describe a method for the estimation of its magnitude in the oceanic mixed layer.

By dimensional reasoning, eddy diffusivity, K, is the product of a turbulent velocity scale, u_*, and a turbulent length scale, λ. Within the lowest 20 or 30 m of the neutrally stable, atmospheric boundary layer (usually called the surface layer, as opposed to the outer or Ekman layer where rotation is important in the dynamics), numerous observations of velocity gradient (wind shear) and Reynolds stress have established that $u_* = u_{*_o} = \sqrt{\tau_o}$ and $\lambda = \kappa z$, where τ_o is the magnitude of kinematic boundary stress, z is height above the surface, and κ is von Kármán's constant (*4*). The results for the atmospheric surface layer cannot be extrapolated directly to the ocean because there is a large disparity in scales between the two boundary layers. A common assumption is that both extend to some proportion of the planetary scale, $u_{*_o}/|f_{cor}|$, where f_{cor} is the Coriolis parameter (*5*), which implies that the governing scales differ roughly by the square root of the density ratio (a factor of about 30). The surface layer in the ocean is thus confined to the upper few meters. The neutrally buoyant outer layer typically extends to 1 to 2 km in the atmosphere and 30 to 60 m in the ocean. Although $\lambda = \kappa|z|$ formulations have been proposed for modeling of the oceanic boundary layer (*6*), numerical boundary layer models based on second-order turbulence closure (*7*) suggest that beyond the first few meters from the ocean surface (that is, beyond the surface layer), the mixing length is no longer proportional to z. Oceanic measurements and theoretical models typically focus on the outer OBL, where there is no widely accepted parameterization of λ and K.

M. G. McPhee, McPhee Research Company, 450 Clover Springs Road, Naches, WA 98937.
D. G. Martinson, Lamont-Doherty Earth Observatory and Department of Geological Sciences, Columbia University, Palisades, NY 10964.

Turbulence in the ocean is usually measured at small scales (for example, with high-frequency shear probes) from which dissipation of turbulent kinetic energy (TKE) is estimated (8). Reynolds stress magnitude is then inferred from some approximation to the TKE equation (9). Analogous techniques exist for the estimation of heat flux from the dissipation of temperature variance (*10*). The methods are controversial, especially regarding the definition of mean gradients, or equivalently, the choice of length scale (*11*). Most oceanic turbulence measurements have been made in the stratified thermocline underlying the mixed layer, where buoyancy and internal waves are important. Scales that depend on the reciprocal of the buoyancy frequency (*12*) are not appropriate for the neutrally stratified or statically unstable mixed layer, nor is $\kappa|z|$ a good choice beyond the first few meters. Thus, to extract flux values from dissipation measurements in the mixed layer, we need either accurate measurement of the mean shear associated with turbulence, or alternatively, the mixing length, λ (*13*).

During ISW-1, we suspended six instrument clusters on a rigid mast spanning 24 m in the mixed layer to measure turbulent heat flux and Reynolds stress. Each cluster measured velocity components u, v, and w along with temperature, T, and conductivity, six times per second. The geometry of the cluster allowed measurement of coherent turbulent eddies down to length scales of ~25 cm (*14*). Turbulence data from the cluster 12 m below the boundary were discarded because of electronic noise contamination in one current component. From day 86.5 (1200 UTC on 26 March 1992) to day 89.0, the ice camp drifted rapidly north in response to a storm with southerly winds. Currents in the mixed layer were relatively steady, and mixed layer depth varied from about 30 to 50 m. Velocity and temperature data were divided into 15-min intervals for the calculation of vertical turbulent fluxes of heat, H, and momentum, $\hat{\tau}$ (*3*).

Scalar gradients in the so-called mixed layer are typically much too small to be detected at the standard calibration accuracy of 0.01°C specified for each thermometer in the instrument clusters. However, the platinum resistance thermometers are capable of much higher resolution, and reasoning that a well-stirred, polar mixed layer with no heat flux is close to an ideal calibration bath, we adjusted the calibrations accordingly (Fig. 1). Using the refined calibrations, we obtained a time series of temperature gradient by linear regression over the vertical extent of the mast each hour. Eddy thermal diffusivity, K_h, was calculated from a linear regression of vertical average kinematic heat flux, $\overline{\langle w'T' \rangle}$, against the negative thermal gradient, $-\partial T/\partial z$, from sample pairs for which the temperature slope was statistically significant (*15*). The heat flux regression slope is $K_h = 0.018 \pm 0.004$ m^2 s^{-1}. Heat flux clearly follows temperature gradient over time, even when the gradient is small (Fig. 1).

The small values of oceanic heat flux, combined with observations of ice temperature showing little heat conduction near the base of the ice (*16*), rule out surface buoyancy flux as a significant factor in OBL dynamics (*17*). Because there was practically no mean density gradient in the upper 24 m, the OBL was neutrally stable with regard to the turbulence dynamics; that is, buoyancy production was insignificant in the TKE equation.

Viewed from a reference frame drifting with the ice, the mean flow velocity (Fig. 2A) rotated counterclockwise with increasing depth. Conceptually, the observed current system may be divided into three components (*18*, *19*), which include (i) the strong shear layer near the surface (corresponding to the atmospheric surface layer), (ii) the frictional Ekman (*20*) spiral, apparent between 4 and 24 m, where rotational effects are paramount (the outer layer), and (iii) a small geostrophic current attributed to sea surface tilt. Although Ekman turning is clearly present in the mean velocity, it is difficult to estimate eddy viscosity directly from the velocity profile because of complications imposed by surface layer shear and geostrophic current. The Reynolds stress profile (Fig. 2B), on the other hand, derives from short-term covariance statistics and is not affected by geostrophic current. We used the Reynolds stress vector measured 4 m below the ice to construct a theoretical profile of turbulent stress on the basis of a simple similarity model (*21*). The model implies that $u_{*_o} = 0.012$ m s^{-1}, from which the eddy viscosity is $K_{sim} = K_* u_{*_o}^2/|f_{cor}| = 0.021$ m^2 s^{-1}, where K_* is a constant nondimensional eddy viscosity. Except for a clockwise deviation of about 30° in measured stress direction at 20 m, modeled stress corresponds closely with observed.

In flows with high Reynolds numbers,

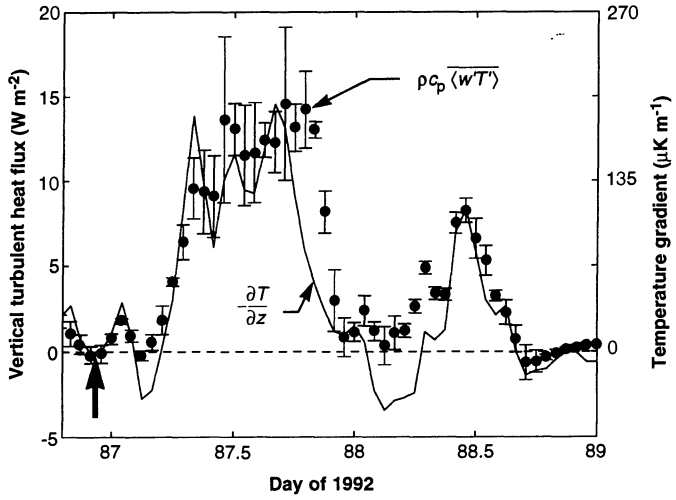

Fig. 1. Time series of vertical turbulent heat flux $\rho c_p \overline{\langle w'T' \rangle}$ (circles, left axis) and temperature gradient (curve, right axis). The overbar indicates a vertical average across five turbulence clusters from 4 to 24 m; error bars are twice the sample standard deviation. The temperature gradient was calculated by linear regression, after the calibration of each thermometer was adjusted by a constant amount to match mixed-layer temperature from the ISW-1 profiling conductivity-temperature-depth (CTD) instrument at day 86.95, when the heat flux was near zero (heavy arrow).

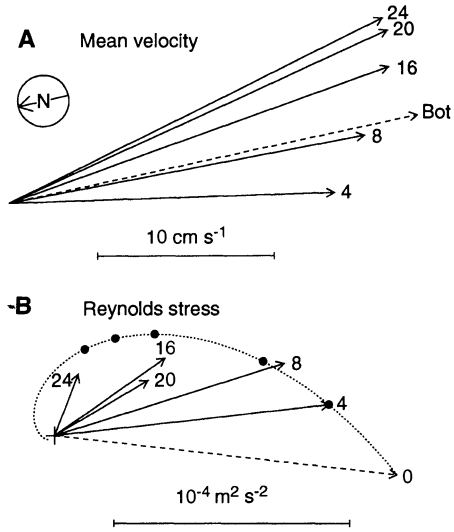

Fig. 2. (**A**) Plan view of mean velocity at five levels, averaged over the storm. Numbers indicate distance in meters from the ice-ocean interface. The dashed vector labeled "Bot" is the apparent velocity of the ocean floor in the drifting reference frame, obtained from satellite navigation. Geostrophic current (that is, the current that would exist in the absence of the drift-induced boundary layer current) is approximately the difference between vectors labeled "24" and "Bot." (**B**) Horizontal Reynolds stress. The dotted stress hodograph is from a similarity model for the rotational boundary layer (*21*). Boundary stress (dashed vector) is inferred from the model solution, which matches measured stress at 4 m.

turbulent transports of momentum and heat depend much more on the characteristics of the overturning eddies than on the respective molecular diffusivities (which differ by an order of magnitude); thus, we expect that eddy viscosity and eddy thermal diffusivity should be roughly the same. Indeed, our estimates of the bulk diffusivities for the boundary layer are $K_h = 0.018\ m^2\ s^{-1}$ and $K_{sim} = 0.021\ m^2\ s^{-1}$.

We also investigated the vertical structure of mixing length and eddy viscosity from measurements at the sampling depths considered separately. Two "spectral" methods based on the measured Reynolds stress and weighted variance spectra of vertical velocity were used. The first method exploits the balance between TKE shear production and dissipation: $\lambda_\varepsilon = u_*^3/\varepsilon$ (*9*, *13*). The definition of friction velocity is local: $u_* = \sqrt{|\hat{\tau}|}$ (*3*). The TKE dissipation is determined from spectral density levels in the inertial subrange (*22*). The method is an inversion of the so-called inertial-dissipation technique used to derive u_{*_o} in the atmospheric surface layer, where λ is obtained from Monin-Obukhov similarity theory (*23*). Here we derive λ from measured Reynolds stress and ε.

The second spectral method makes no assumptions about the TKE equation but relies instead on the wave number at the peak of the weighted w spectrum (k_{max}). In the atmospheric surface layer, it has been shown that k_{max} varies inversely with distance from the surface (*24*) and is thus also inversely proportional to λ. In the outer part of the under-ice OBL, $1/k_{max}$ no longer scales with $|z|$, but a working hypothesis is that the spectral peak does still indicate the size of the dominant eddies: that is, $\lambda_{peak} = c_\lambda/k_{max}$ (*25*).

Vertical velocity spectra were averaged over 6 hours at all levels and consistently showed a region with $-2/3$ logarithmic slope (for the weighted spectra) indicative of the inertial subrange (Fig. 3). When averaged over the storm (2.5 days), mixing lengths calculated from the inverse of the peak wave numbers are similar to those inferred from an assumed balance of TKE production with dissipation and vary from 2 to 3 m through much of the boundary layer (Fig. 4A). The distribution is clearly different from that derived from surface layer scaling, $\lambda = \kappa|z|$, and is a strong indication that below the first few meters, the maximum size of the turbulent eddies is not controlled by distance from the boundary. A depth-dependent distribution of eddy viscosity (K_{local}), calculated by the combination of the measured Reynolds stress magnitude (Fig. 4B) with the spectral peak estimate for λ, agrees reasonably well with the bulk eddy viscosity K_{sim} (Fig. 4C). The vertically averaged value of K_{local} is $0.019\ m^2\ s^{-1}$.

Because the Ekman solution for stress decreases exponentially from the interface, the eddy viscosity may also be estimated (*26*) from the fitted extinction coefficient, a, according to $K_{fit} = |f_{cor}|/(2a^2)$ (this differs from K_{sim} because only one measurement at 4 m was used to derive the similarity stress profile). The value of K_{fit} is sensitive to small stress in the deep boundary layer; its value is $0.020\ m^2\ s^{-1}$ if the bottommost cluster is deleted from the semilogarithmic regression analysis.

Our results show that provided there are no other important sources or sinks of TKE in the boundary layer, bulk eddy viscosity and eddy thermal diffusivity in the mixed layer are similar and are well estimated by $K = 0.02\tau_o/|f_{cor}|$. This is consistent with earlier findings evident from direct turbulence measurements and inferred from ice drift statistics (*19*, *25*, *27*) and underscores the similarity between outer boundary layers in the atmosphere and ocean. We also found that the peak in the vertical velocity spectrum provides a good estimate of the turbulent mixing length. If this concept withstands further experimental scrutiny, it provides a fairly easy observational test for numerical models and a straightforward means for the determination of flux from dissipation measurements in well-mixed boundary layers, from both temperate and polar oceans.

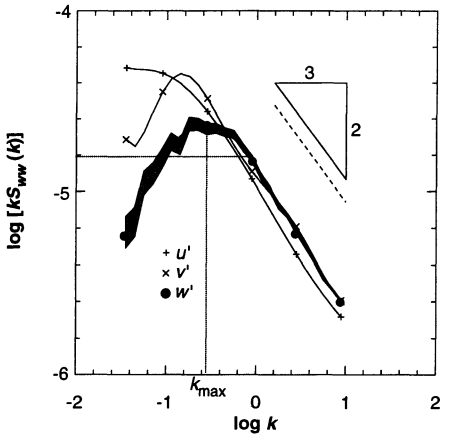

Fig. 3. Examples of 6-hour-average spectra from the 20-m turbulence cluster at day 86.87. The power spectra were calculated from 1-hour time series of the longitudinal (u'), horizontal cross-stream (v'), and vertical (w') deviatory components, then fitted with seventh-order polynomials in wave number $k = 2\pi f/\langle U\rangle$, where f is frequency and $\langle U\rangle$ is mean flow speed. The envelope surrounding the polynomial fit to the w' spectrum shows the 95% confidence interval for spectral estimates averaged in wave number bins. In an isotropic, inertial subrange, the weighted spectra decrease with a $-2/3$ slope in the log-log representation, with cross-stream and vertical spectral levels being 4/3 of longitudinal (*22*). The inertial subrange slope and spectral separation are indicated by the triangle and dashed line, respectively. Dotted lines mark the spectral peak, $k_{max} = c_\lambda/\lambda_{peak}$ (vertical) and the spectral level used to estimate dissipation (horizontal). Dissipation may be estimated at any point in the $-2/3$ slope region.

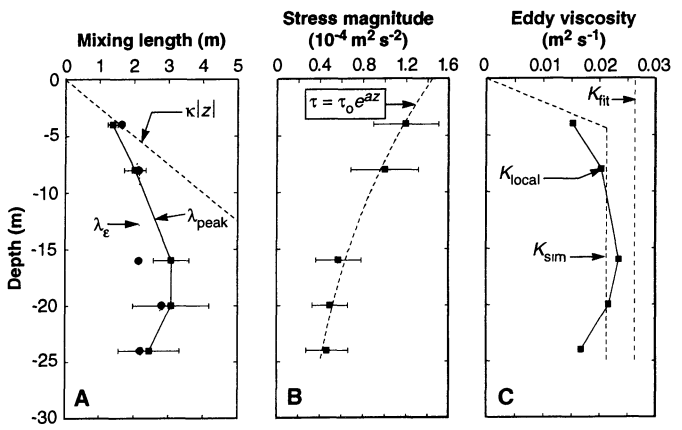

Fig. 4. (**A**) Mixing length determined by assuming shear production equals dissipation (λ_ε) and from the inverse of the wave number at the peak in the weighted spectrum (λ_{peak}). Error bars on the spectral peak estimate indicate twice the sample standard deviation over time; those for the dissipation estimate are similar but not plotted. (**B**) Average Reynolds stress magnitude, with a least squares–fitted exponential decay with depth. The coefficients are $\tau_o = 1.44 \times 10^{-4}\ m^2\ s^{-2}$ and $a = 0.051\ m^{-1}$. (**C**) Eddy viscosities: K_{sim}, calculated from the similarity solution (Fig. 2B), except with a linear increase with depth in the surface layer; $K_{local} = u_*\lambda_{peak}$; and K_{fit}, calculated from the extinction coefficient, a.

REFERENCES AND NOTES

1. Ocean Studies Board, National Research Board, "Oceanography in the Next Decade" (National Academy of Sciences, Washington, DC, 1992).
2. A. L. Gordon and Ice Station Weddell Group of Principal Investigators and Chief Scientists, *Eos* **74**, 121 (1993).
3. Turbulent heat flux is $H = \rho c_p\langle w'T'\rangle$, where angle brackets indicate ensemble averaging, approximated by the zero-lag covariance over a 15-min averaging interval; ρ is density, c_p is specific heat, and w' and T' are deviatory (mean removed in each 15-min averaging interval) vertical velocity and temperature, respectively. Kinematic Reynolds stress (stress divided by density) is $\hat{\tau} = \langle u'w'\rangle + i\langle v'w'\rangle$, expressed as a complex number with real component toward the east and imaginary component north.
4. J. A. Businger, J. C. Wyngaard, Y. Izumi, E. F. Bradley, *J. Atmos. Sci.* **28**, 181 (1971).
5. C.-G. Rossby and R. B. Montgomery, *The Layer of Frictional Influence in Wind and Ocean Currents*, vol. 3, no. 3 of *Papers in Physical Oceanography and Meteorology* (Massachusetts Institute of Technology and Woods Hole Oceanography Institution, Cambridge, MA, 1935); A. K. Blackadar

and H. Tennekes, *J. Atmos. Sci.* **25**, 1015 (1968).
6. O. S. Madsen, *J. Phys. Oceanogr.* **7**, 248 (1977); J. E. Weber and A. Melsom, *ibid.* **23**, 193 (1993).
7. G. L. Mellor and T. Yamada, *Rev. Geophys.* **20**, 851 (1982).
8. See, for example, reviews by M. L. Gregg [*J. Geophys. Res.* **92**, 5249 (1987)] and E. J. Hopfinger [*ibid.*, p. 5287]. Most of the reported turbulence measurements are from the stratified thermocline below the mixed layer, but see also T. J. Shay and M. C. Gregg [*J. Phys. Oceanogr.* **16**, 1777 (1986)] for dissipation measurement in a convecting mixed layer.
9. The steady TKE equation for a high Reynolds number, horizontally homogeneous, incompressible flow [H. Tennekes and J. L. Lumley, *A First Course in Turbulence* (MIT Press, Cambridge, MA, 1972), p. 97] is typically further simplified by neglect of spatial transport terms, leading to a balance among three terms where

$$P_s + P_b = \varepsilon$$

where

$$P_s = -\left(\langle u'w'\rangle\frac{\partial U}{\partial z} + \langle v'w'\rangle\frac{\partial V}{\partial z}\right)$$

is TKE shear production

$$P_b = -\frac{g}{\rho}\langle\rho'w'\rangle = -\langle b'w'\rangle$$

is the TKE production by gravitational body forces ($\langle b'w'\rangle$ is the turbulent buoyancy flux), and

$$\varepsilon = \nu\left\langle\frac{\partial u'_j}{\partial x_i}\frac{\partial u'_j}{\partial x_i}\right\rangle$$

is TKE dissipation into heat (ν is kinematic molecular viscosity and repeated indices imply summation). In a neutrally stratified flow, buoyancy production is negligible.
10. H. Tennekes and J. L. Lumley, in (*9*), p. 98.
11. C. H. Gibson, *J. Geophys. Res.* **92**, 5383 (1987); A. Gargett, *ibid.* **95**, 15971 (1990); J. N. Moum, *J. Phys. Oceanogr.* **20**, 1980 (1990).
12. T. M. Dillon, *J. Geophys. Res.* **87**, 9601 (1982).
13. From the simplified TKE equation with no buoyancy flux, assuming that mean shear and stress are aligned in the x direction, $-\langle u'w'\rangle\partial U/\partial z = u_*^3/\lambda = \varepsilon$.
14. M. G. McPhee, *J. Geophys. Res.* **97**, 5365 (1992).
15. If m is the slope of a linear regression of y against x (temperature against depth) for five instrument clusters, m is significantly different from zero at the 95% confidence level provided

$$\left|\frac{m}{s_{y|x}\sqrt{1/\sum_{i=1}^{5}(x_i - \bar{x})^2}}\right| \geq t_{0.025|3}$$

where $s_{y|x}$ is an estimate of variability about the line, and $t_{0.025|3}$ is the 2.5 percentage point of Student's t distribution for three degrees of freedom, assuming the temperature samples are drawn from a population with independent, normally distributed errors with common variance [A. H. Bowker and G. J. Lieberman, *Engineering Statistics* (Prentice-Hall, Englewood Cliffs, NJ, 1959), p. 255]. Of 61 hourly samples in the period 86.5 to 89.0, 32 temperature gradients were statistically significant. In the subsequent regression of measured heat flux against temperature gradient, similar analysis leads to a 95% confidence interval for the regression slope (K_h) of 0.014 to 0.022. The correlation coefficient is 0.85.
16. S. Ackley, personal communication.
17. A measure of the effect of surface buoyancy flux is the Obukhov length $L = u_{*o}^3/(\kappa\langle w'b'\rangle_o)$. When the magnitude of L is comparable to, or less than, other turbulent length scales in the flow, buoyancy is dynamically important. This early in the season, most of the heat conducted to the atmosphere from the ice comes from cooling and freezing within the ice column, hence, there is little conduction near the bottom (*16*), and upward oceanic heat flux causes melting at the ice-ocean interface. Melting associated with a heat flux of 20 W m^{-2} is roughly 6 mm per day, and fresh water released by such melting would produce a stabilizing surface buoyancy flux of about $\langle w'b'\rangle_o = 1.3 \times 10^{-8}$ m^{-2} s^{-3} (*14*). With a mean value of 0.012 m s^{-1} for u_{*o}, the Obukhov length is about 300 m, far too large to be dynamically important. Even if there were a linear temperature gradient in the ice, so that freezing would produce destabilizing buoyancy flux, its magnitude would be insignificant under thick ice surrounding the instrument mast.
18. K. Hunkins, *Deep-Sea Res.* **13**, 607 (1966).
19. M. G. McPhee, in *Polar Oceanography*, W. Smith, Ed. (Academic Press, San Diego, CA, 1990), vol. 1, chap. 6.
20. V. W. Ekman, *Ark. Mat. Astron. Fys.* **2**, 1 (1905).
21. M. G. McPhee, *Boundary-Layer Meteorol.* **21**, 325 (1981). The model expresses nondimensional turbulent stress as a complex exponential $\hat{T} = e^{\delta\zeta}$, where $\hat{\tau} = \hat{\tau}/(u_{*o}\hat{u}_{*o})$; $\hat{\tau}$ is the horizontal, kinematic stress vector; $\delta = (1 - i)/\sqrt{2K_*}$ is a complex attenuation constant; and $\zeta = |f_{cor}|z/(u_{*o}\eta_*)$ is the nondimensional vertical coordinate. In the theory, K_*, the nondimensional eddy viscosity, is a constant with numerical value about 0.02, and η_* is a stability factor, equal to one if the flow is neutrally stable.
22. J. O. Hinze, *Turbulence* (McGraw-Hill, New York, ed. 2, 1975), chap. 3. In a turbulent shear flow that is anisotropic at large scales, it is often possible to identify a wave-number band at smaller scales where turbulence is nearly homogeneous and isotropic and TKE is neither produced nor dissipated. In the so-called inertial subrange, a simple power law describes the spectrum

$$S_{ww} = \frac{4}{3}\alpha_\varepsilon\varepsilon^{2/3}k^{-5/3}$$

where k is the wave number in radians per meter, $S_{ww}(k)$ is the power spectral density of the vertical velocity at k, and α_ε is the Kolmogorov constant, taken here to be 0.52.
23. J. B. Edson, C. W. Fairall, P. G. Mestayer, S. E. Larsen, *J. Geophys. Res.* **96**, 10689 (1991).
24. N. E. Busch and H. A. Panofsky, *Q. J. R. Meteorol. Soc.* **94**, 132 (1968). In our notation, their expression for the nondimensional vertical wind spectrum in the surface layer is

$$\frac{kS_{ww}(k)}{u_{*o}^2} = \frac{A(\omega/\omega_m)}{1 + 1.5(\omega/\omega_m)^{5/3}}$$

with $\omega = kz/(2\pi)$. They did not find similar simple expressions for the downstream or horizontal cross-stream spectra. They estimated the constants to be $A = 1.075$ and $\omega_m = 0.32$, where the latter is the nondimensional wave number at the peak in the spectrum and implies a value of 0.8 for $c_\lambda = \lambda_{peak}k_{max}$. Using our data from 4 m, assuming that surface-layer scaling held approximately at that depth, we found a better fit to the mean spectrum with a slightly higher value for ω_m, from which $c_\lambda = 0.85$.
25. M. G. McPhee and J. D. Smith, *J. Phys. Oceanogr.* **6**, 696 (1976).
26. Differentiation with respect to z of the steady Ekman (*20*) momentum equation with the substitution $\hat{\tau} = K\partial\hat{U}/\partial z$, yields $(if_{cor}/K)\hat{\tau} = d^2\hat{\tau}/dz^2$, with solution $\hat{\tau} = \hat{\tau}_o e^{a(1-i)z}$ (southern hemisphere) where $a = \sqrt{|f_{cor}|/(2K)}$.
27. M. G. McPhee, *J. Phys. Oceanogr.* **9**, 388 (1979).
28. This research was funded by the Office of Polar Programs, National Science Foundation (grants OPP9110422 and OPP9025083) and by the Office of Naval Research (contract N00014-84-C-0028). We thank R. Andersen and T. Baker for excellent field support and V. Lukin and J. Ardai for scientific and logistic support. The CTD data were kindly supplied by A. Gordon and B. Huber. Lamont-Doherty Earth Observatory contribution 5143.

23 August 1993; accepted 5 November 1993

Root-Knot Nematode–Directed Expression of a Plant Root–Specific Gene

Charles H. Opperman, Christopher G. Taylor, Mark A. Conkling*

Root-knot nematodes are obligate plant parasites that induce development of an elaborate feeding site during root infection. Feeding-site formation results from a complex interaction between the pathogen and the host plant in which the nematode alters patterns of plant gene expression within the cells destined to become the feeding site. Expression of *TobRB7*, a gene expressed only in tobacco roots, is induced during feeding site development. The cis-acting sequences that mediate induction by the nematode are separate from those that control normal root-specific expression. Reporter transgenes driven by the nematode-responsive promoter sequences exhibit expression exclusively in the developing feeding site.

Plant parasitic nematodes are among the most devastating pathogens of the world's food crops, causing an estimated $77 billion in food and fiber crop losses in 1987. The majority of this loss is caused by the root-knot nematodes (*Meloidogyne* spp.) (*1*). Root-knot nematodes are obligate sedentary endoparasites with a complex and intimate relationship with their host plants. The nematodes have a host range exceeding 2000 plant species (*2*). The primary symptom of root-knot nematode infection is the formation of enlarged galls on roots of susceptible host plants. Nutrient and water uptake are substantially reduced because of the damaged root system, resulting in weak and poor-yielding plants.

Nematode growth and reproduction depend on establishment of modified feeding sites within the plant root. The infective second-stage juvenile nematode (J2) moves freely through the soil. The J2 penetrates the root intercellularly in the region just posterior

C. H. Opperman, Department of Plant Pathology, North Carolina State University, Raleigh, NC 27695–7616.
C. G. Taylor and M. A. Conkling, Department of Genetics, North Carolina State University, Raleigh, NC 27695–7614.

*To whom correspondence should be addressed.